DSC-Vol. 58, Proceedings of the ASME Dynamics Systems
and Control Division
ASME 1996

Estimation and Modeling of Human Hand Impedance During Isometric Muscle Contraction

Toshio TSUJI and Makoto KANEKO

Industrial and Systems Engineering,
Hiroshima University
1-4-1, Kagamiyama, Higashi-Hiroshima, 739 Japan
E-mail: tsuji@huis.hiroshima-u.ac.jp

ABSTRACT

The present paper examines human hand impedance characteristics with consideration of effects of muscle activity. While a subject maintains a given hand location with a specified muscle activation level or a hand force, small external disturbances are applied to his hand. The corresponding force-displacement vectors are measured to estimate the hand impedance by means of a second-order linear model. The main results of the experiments can be summarized as follows: (1) geometrical parameters of the hand stiffness and viscosity ellipses change depending on the muscle activation levels of the subjects, (2) both the stiffness and the virtual equilibrium point of the subject's hand change depending on the amplitude of the generated hand force, and (3) hand stiffness and viscosity can be predicted from the joint angles and EMG signals of the subject's arm.

INTRODUCTION

Understanding the impedance characteristics of the human arm has lately attracted considerable attention not only in the biological field, but also in the robotics field. For the multi-joint arm movements, Mussa-Ivaldi et al. (1985) developed an experimental method to measure human hand stiffness while maintaining posture. They found that the hand stiffness systematically depended on the arm postures, and that the subjects could not regulate the orientations and shapes of the stiffness ellipses. Flash and Mussa-Ivaldi (1990) showed that the spatial variations of the hand stiffness ellipses in the horizontal plane could be explained by a covariation between the shoulder stiffness and the stiffness component provided by two-joint muscles. Then, Dolan et al. (1993) and Tsuji et al. (1995) extended the experimental method developed by Mussa-Ivaldi et al. (1985) to include measurement of dynamic components such as viscosity and inertia as well as stiffness.

On the other hand, it is well known that the viscoelastic property of skeletal muscles (Dowben, 1980) and the sensitivity of the proprioceptive feedback in the stretch reflex pathway (Houk, 1979), which are major sources of the human hand viscoelasticity, largely change depending on activation levels of the muscles. Tsuji et al. (1994) pointed out that muscle contraction for a grip force increases the hand stiffness and viscosity, because greater voluntary muscle activation is responsible for higher muscle viscoelasticity. Also, Gomi et al. (1992) estimated hand stiffness during two joint arm movements and argued that dynamic stiffness is different from the static one because of the different neuromuscular activity during movements. Although importance of variable structure of impedance characteristics regulated by a motor command from the central nervous system (CNS) has been pointed out as mentioned above, the previous investigators did not analyze a variation of the hand impedance characteristics under different muscle activation levels.

The present paper analyzes the spatial characteristics of the human hand impedance with consideration of effects of the muscle activity. In order to examine these effects experimentally, two different experimental conditions are chosen: 1) maintaining the hand force in different values and directions under a specific arm posture and 2) maintaining the muscle activity in different levels under a specific arm posture. Then, the human hand impedance is estimated and its spatial features such as size, orientation and shape are examined. Finally, a human arm impedance model including postural and muscular effects is developed.

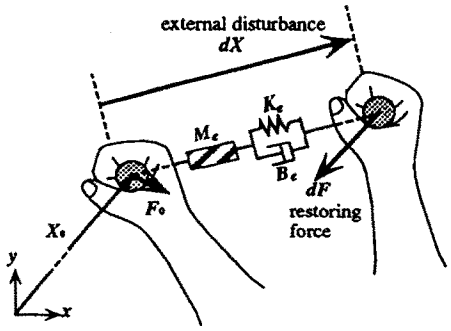

Fig. 1 Description of hand impedance for small motions around an equilibrium posture

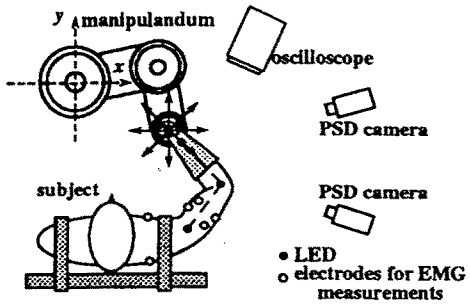

Fig. 2 Subject and manipulandum

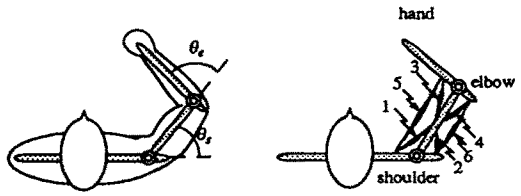

Fig. 3 Upper limb model

ESTIMATION OF HUMAN HAND IMPEDANCE

Impedance Model

The following hand impedance model is assumed in the end-point level:

$$M_e(t)\ddot{X}(t) + B_e(t)\dot{X}(t) + K_e(t)(X(t) - X_v(t)) = -F(t), \quad (1)$$

where $X(t) \in \Re^l$ is the hand position vector; $F(t) \in \Re^l$ is the force vector exerted by the hand to the environment; $X_v(t) \in \Re^l$ represents a virtual equilibrium point (or a virtual trajectory); and $M_e(t)$, $B_e(t)$ and $K_e(t) \in \Re^{l \times l}$ represent hand inertia, viscosity and stiffness matrices, respectively. $M_e(t)$ is the equivalent inertia evaluated in the task space, which must be strongly dependent upon arm postures. The hand viscosity $B_e(t)$ and hand stiffness $K_e(t)$ also depend on the viscoelastic properties of skeletal muscles, low-level neural reflexes and passive elements such as skins and veins.

In order to estimate the hand impedance, the hand of the subject is displaced from an equilibrium by means of a small disturbance with short duration (Fig. 1). This kind of the disturbance is necessary in order to assume the approximate constancy of M_e, B_e and K_e. As a result, hand inertia, viscosity and stiffness are assumed to be constant after the onset of the disturbance. Then we can limit ourselves to a constant parameter, second order, linear impedance model of the hand dynamics for small motions:

$$M_e\ddot{X}(t) + B_e\dot{X}(t) + K_e(X(t) - X_v(t)) = -F(t). \quad (2)$$

Also, since at the onset time t_0 of the disturbance we have

$$M_e\ddot{X}(t_0) + B_e\dot{X}(t_0) + K_e(X(t_0) - X_v(t_0)) = -F(t_0), \quad (3)$$

we can get

$$M_e d\ddot{X}(t) + B_e d\dot{X}(t) + K_e dX(t) - K_e(X_v(t) - X_v(t_0)) = -dF(t), \quad (4)$$

where $dX(t) \equiv X(t) - X(t_0)$ and $dF(t) \equiv F(t) - F(t_0)$.

In the present paper, the virtual trajectory $X_v(t)$ is assumed not to change in a complex way after the onset of the disturbance, since the disturbance is applied in short duration. Then, when the virtual trajectory is assumed to change with a constant velocity as a first-order approximation, we can have

$$X_v(t) = (t - t_0)c + X_v(t_0), \quad (5)$$

where $c \in \Re^l$ is a constant velocity vector of the virtual trajectory. Substituting (5) into (4) yields

$$M_e d\ddot{X}(t) + B_e d\dot{X}(t) + K_e dX(t) - (t - t_0)K_e c = -dF(t). \quad (6)$$

If the specific external disturbance pattern with $dX(t_f) = d\dot{X}(t_f) = d\ddot{X}(t_f) = 0$ that returns to the initial hand position at time t_f is chosen, we can derive

$$K_e c = \frac{dF(t_f)}{t_f - t_0}. \quad (7)$$

Consequently, the following hand impedance model can be obtained:

$$M_e d\ddot{X}(t) + B_e d\dot{X}(t) + K_e dX(t) = -dF_d(t), \quad (8)$$

where

$$dF_d(t) = dF(t) - \frac{t - t_0}{t_f - t_0} dF(t_f). \quad (9)$$

The above equation means that the difference between the hand forces at t_0 and t_f reduces to a change of the virtual trajectory. In the present paper, the hand impedance matrices M_e, B_e, K_e are estimated using (8).

Experiments

Figure 2 shows experimental apparatus for hand impedance estimation (Tsuji et al., 1995). A two-joint planar direct drive robot was used as a manipulandum. The force vector between the hand and the handle was measured by a force sensor attached to the robot handle and the arm posture of the subject was measured by a stereo-PSD camera system (for details, see Tsuji et al., 1995).

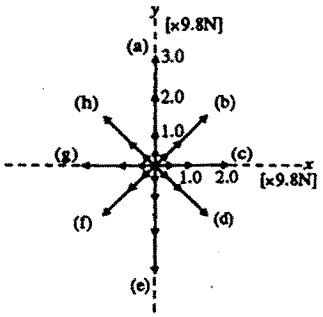

Fig. 4 The target hand forces

During experiments, surface EMG signals were measured from m. pectoralis major (a single-joint flexor acting on the shoulder joint, which is represented as muscle 1 in Fig. 3), m. infraspinatus (a single-joint extensor acting on the shoulder joint represented as muscle 2), m. brachialis (a single-joint flexor acting on the elbow joint represented as muscle 3), m. triceps brachii caput laterale (a single-joint extensor acting on the elbow joint represented as muscle 4), m. biceps brachii caput longum (a two-joint flexor represented as muscle 5) and m. triceps brachii caput longum (a two-joint extensor represented as muscle 6) in order to estimate activation levels of the muscles. After rectification and smoothing by the second order Butterworth filter (cut-off frequency 1 Hz), the EMG signal measured from each muscle was normalized for a value in the maximum voluntary contraction (MVC) of the muscle, which was defined as a muscle activation level α_i ($0.0 \leq \alpha_i \leq 1.0$, $i = 1, \cdots\}$, 6).

Under the experimental setup mentioned above, two different sets of the experiments were carried out.

1) *Maintaining hand force* The force vector $F(t)$ exerted by the subject's hand to the handle was displayed on the oscilloscope, and the subject was asked to keep the hand force to the instructed direction and amplitude. The target hand force was set to 0.5, 1.0 and 2.0 (×9.8 N) along eight directions shown in Fig. 4. Also, the additional amplitude 3.0 (×9.8 N) was used along y-axis.

2) *Maintaining muscle activation level* A mean value of the measured activation levels of the flexor and extensor of the two-joint muscles was displayed on the oscilloscope. The subject was asked to maintain the initial hand position while keeping the mean value of the muscle activation levels to a target value. The target muscle activation level was set to seven different values (0, 5, 10, ..., 30 percents of the MVC).

In experiment 2), both the flexor and extensor are activated simultaneously, while one of them is mainly activated in experiment 1). The posture (θ_s = 1.04 rad, θ_e = 1.57 rad) shown in Fig. 3 was used as the nominal one. Also, the muscle activation level and the hand force vector were not presented to the subjects after the onset of the disturbance in order to avoid any effects of the visual feedback.

Five sets of the experiments for each experimental conditions explained above, where each set includes data corresponding to eight different disturbances, were performed in one day to avoid fatigue of the subject. And this session of the experiments were repeated six days for each subject.

ESTIMATED HUMAN HAND IMPEDANCE

Four male subjects, 21 - 23 years old were examined for both experiment. Figure 5 shows an example of the measured hand displacement $dX(t)$, velocity $d\dot{X}(t)$, acceleration $d\ddot{X}(t)$, and force $dF_d(t)$ in experiment 2), where the target muscle activation level is 10 percent of the MVC. The measured time history of the displacement $dF_d(t)$ (solid lines) well agrees with the predicted value (dashed lines) which is computed by (8) with the estimated hand impedance. The multiple correlation coefficient between the measured and predicted values is 0.979. This means that, under our experimental conditions, the hand dynamics of the subject is well approximated by the second-order linear impedance model of (8).

The impedance ellipses corresponding to the symmetrical components of the mean values of the estimated impedance matrices for ten data sets of experiment 1) are shown in Fig. 6, 7, 8, which are arranged according to the eight different directions of the target hand force in each figure (see Fig. 4). The stiffness and viscosity ellipses in Fig. 6 and 7, show that the area, orientation and shape of the ellipses change depending on the target hand force even if the arm posture does not change. The dotted ellipse in Fig. 8 represents the hand inertia computed from the motion equation of the two-link arm model. It can be seen from the figures that the stiffness and viscosity ellipses change largely while a large variation is not observed for the inertia ellipse. It should be noted that the characteristics of the hand impedance found here were also observed similarly for other subjects.

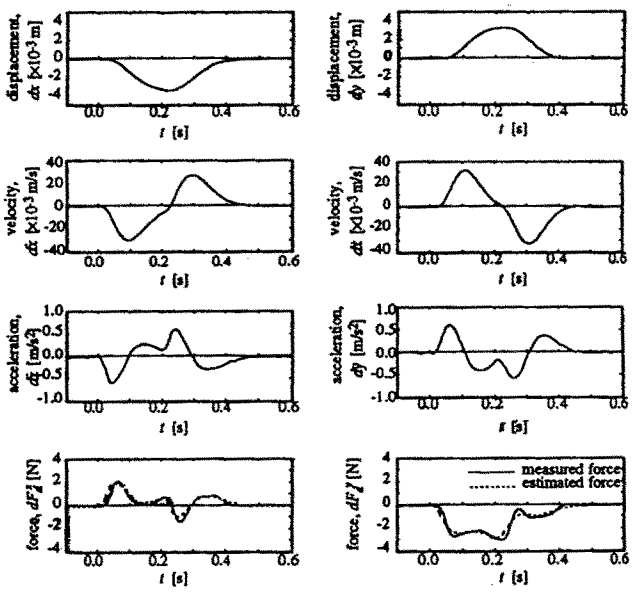

Fig. 5 Example of measured human hand motion and force in experiment 2), where the target activation level was 10 percent of the MVC

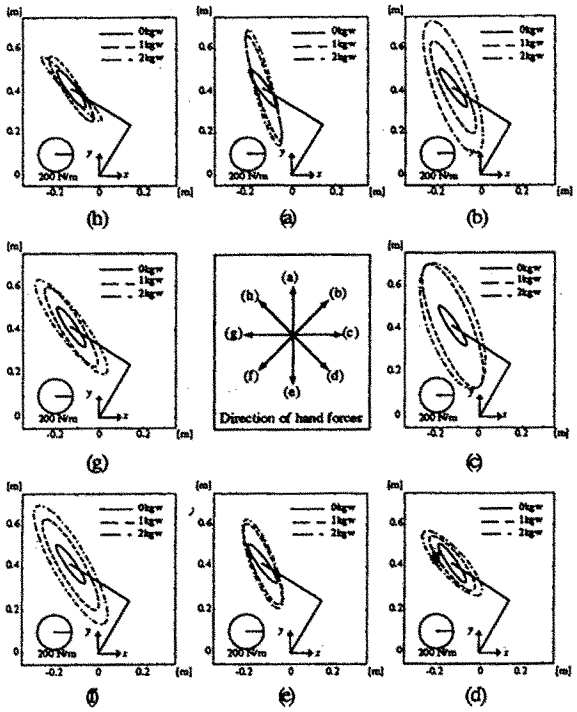

Fig. 6 Changes of stiffness ellipses with direction and amplitude of the target hand forces

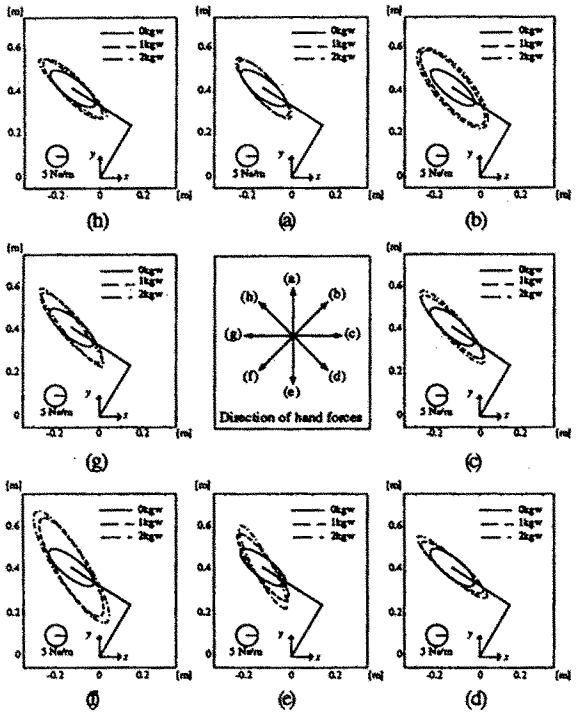

Fig. 7 Changes of viscosity ellipses with direction and amplitude of the target hand forces

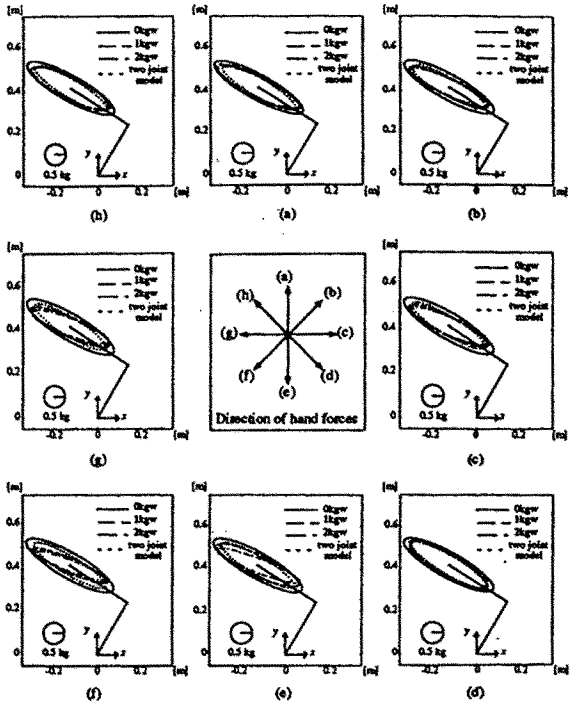

Fig. 8 Changes of inertia ellipses with direction and amplitude of the target hand forces

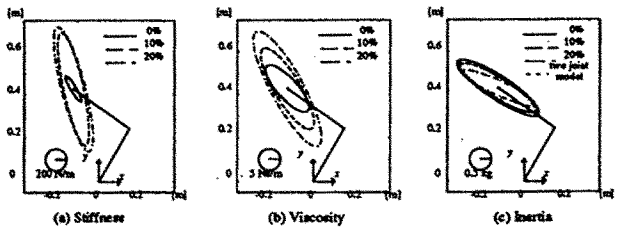

Fig. 9 Changes of impedance ellipses with target muscle contraction levels

Next, a change of the impedance ellipses of a subject with the target muscle activation level is shown in Fig. 9. The solid, dashed, and alternate long and short dashed ellipses represent the mean values of ten data sets of the experimental results corresponding to the target muscle activation levels of 0, 10, 20 percents of the MVC, respectively. Although the exerted force to the handle by the hand is almost zero, the internal force of the arm via muscle co-contraction increases the hand viscoelasticity.

SPATIAL CHARACTERISTICS OF VISCOELASTIC ELLIPSES

Fig. 10 shows the change of the area S of the stiffness ellipses in experiment 1). The vertical axis of each figure represents the area S and the horizontal axis indicates the Euclidean norm of the measured hand force $\|F\|$. For all directions of the hand force, the area of the stiffness ellipse increases almost

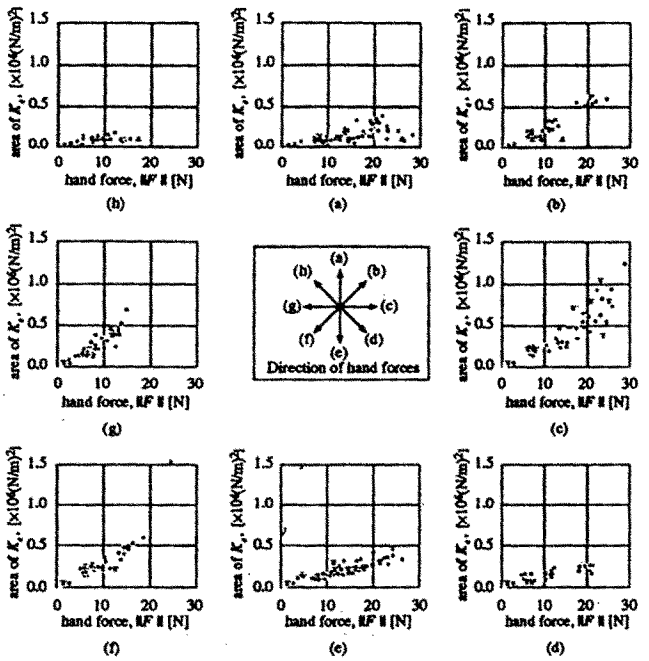

Fig. 10 Area of stiffness ellipses depending on the hand forces

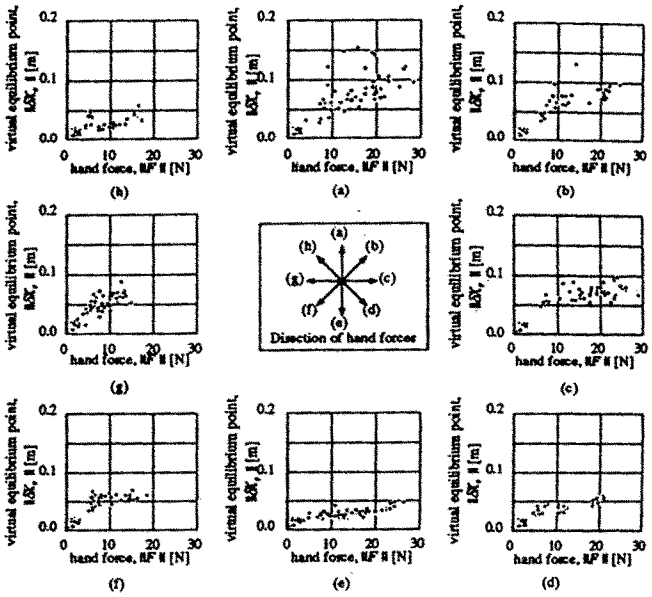

Fig. 11 Amplitude of virtual equilibrium points depending on the hand forces

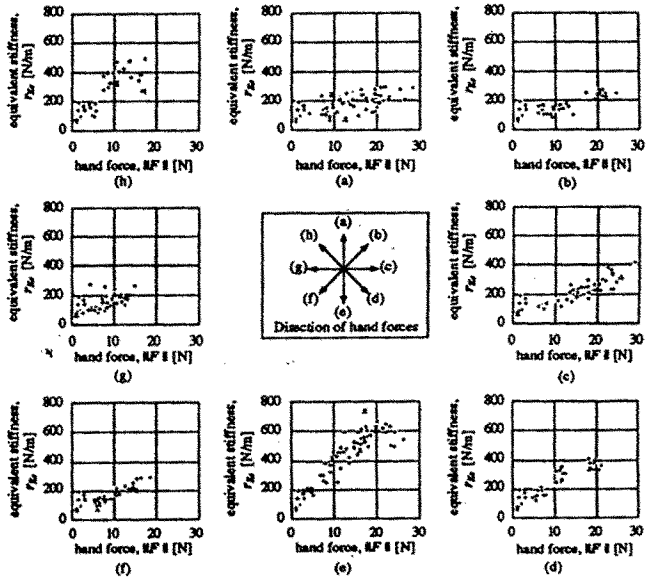

Fig. 12 Amplitude of equivalent stiffness depending on the hand forces

in proportion to the amplitude of the hand force, while the increasing rate of the area is varied depending on the direction of the hand force. It seems that the change of the area while applying the hand force along the direction of the major axis of the stiffness ellipse (Fig. 10 (a), (d), (e), (h)) may be smaller than the one while applying the hand force along the direction of the minor axis (Fig. 10 (b), (c), (f), (g)).

While the hand force is maintained, the relationship between the hand force vector and the virtual equilibrium point at the onset time $t = t_0$ of the disturbance is given as

$$F(t_0) = K_e\,(X_v(t_0) - X(t_0)) \equiv K_e\,\delta X_v(t_0), \qquad (10)$$

where $\delta X_v(t)$ denotes the displacement from the actual hand position $X(t)$ to the virtual equilibrium point $X_v(t)$. Since the hand position $X(t_0)$ is constant, it is easy to generate a large hand force in the direction that the hand stiffness K_e has a large value. In other words, it is not necessary to increase the hand stiffness much while the hand force is applied along the direction of the major axis of the stiffness ellipse. On the other hand, the hand stiffness should be increased in order to generate the hand force easily while it is applied along the direction of the minor axis of the stiffness ellipse.

It can be seen from (10) that the hand stiffness and/or the virtual equilibrium position should be changed in order to regulate the hand force at $t = t_0$. **Figure 11** shows the change of the virtual equilibrium points computed from (10) using the hand force and the hand stiffness measured in experiment 1), which corresponds to Fig. 10. In the figure, the horizontal axis represents the amplitude of the hand force, $\|F\|$, and the vertical axis represents the distance from the hand position to the virtual equilibrium point at $t = t_0$, $\|\delta X_v\|$. The distance from the hand position to the virtual equilibrium point increases, as the hand force becomes large.

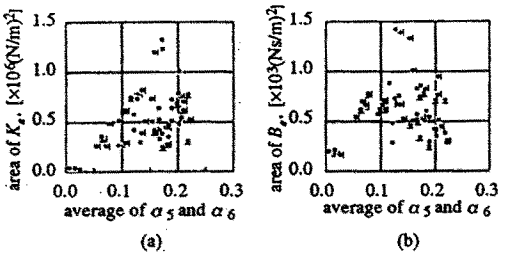

Fig. 13 Area of impedance ellipses depending on the muscle contraction levels

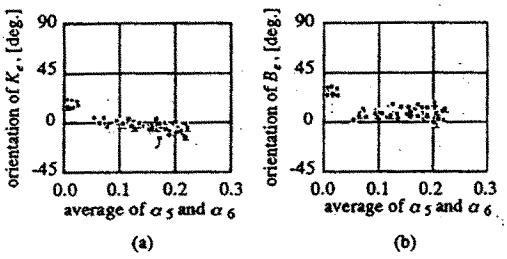

Fig. 14 Orientation of impedance ellipses depending on the muscle contraction levels

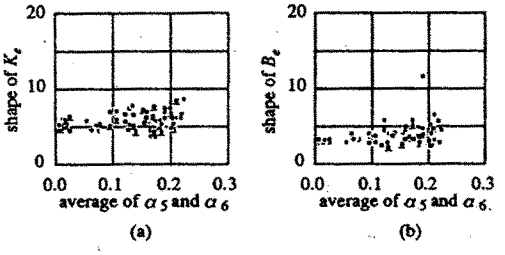

Fig. 15 Shape of impedance ellipses depending on the muscle contraction levels

Then the change of the hand stiffness in this case is examined. Although the changes of the stiffness ellipses have been represented in Fig. 10, even the same stiffness ellipse has a different effect on the generated hand force vector depending on its direction. Therefore, an effective stiffness in the direction of the hand force is defined as a ratio of the virtual equilibrium displacement to the amplitude of the hand force $r_{K_e} = \|F\| / \|\delta X_v\|$, and the change of the effective stiffness is shown in Fig. 12. From the figure, the effective stiffness r_{K_e} increases significantly, as the hand force increases along the corresponding direction. Both the virtual equilibrium point and the stiffness of the subject's hand change simultaneously when the subject regulates the amplitude of the hand force.

Next, Fig. 13 shows a change of the area of the hand viscoelastic ellipses of subject C in experiment 2). The vertical axis represents the area of the ellipses, and the horizontal axis indicates the mean values of the measured activation levels of the flexor and extensor of the two-joint muscles, α_5 and α_6, which represents a co-contracting activity of the flexor and extensor of the upper limb. The area of the stiffness and viscosity ellipses tends to increase, as the muscle activation level increases. The variability observed in the figure is mainly caused by indicating the experimental results measured in five different days simultaneously and the accuracy of the EMG measurements.

Also, the variations of the orientation and shape parameters are shown in Fig. 14 and 15, respectively. The orientation of the stiffness and viscosity ellipses (Fig. 14) changes largely in a clockwise direction at first, then almost maintains the constant value afterwards, as the muscle activation level increases. On the other hand, for the shape of the stiffness and viscosity ellipses (Fig. 15), any definite relation with the muscle activation level is not found in this experimental condition.

MODELING HUMAN ARM IMPEDANCE

Muscle Impedance Model

Using kinematic relationships among the muscle, joint and end-point movements, the transformations of the stiffness matrices can be written as Mussa-Ivaldi (1986).

$$K_j = J^T K_e J \tag{11}$$

$$= G^T K_m G, \tag{12}$$

where $K_e \in \Re^{kl}$, $K_j \in \Re^{m\times m}$, $K_m \in \Re^{n\times n}$ are the stiffness matrices in the end-point, joint and muscle levels, respectively. Also, $J \in \Re^{k\times m}$ and $G \in \Re^{n\times m}$ are the Jacobian matrices.

From (11), the joint viscoelastic matrices can be computed from the corresponding hand impedance estimated experimentally. In this section, the relationship between the joint and muscle stiffness are analyzed based on (12). It should be noted that the viscosity analysis will be also held in the same manner.

The Jacobian matrix G and the muscle stiffness matrix K_m included in (12) are represented as follows:

$$G = \begin{pmatrix} -d_{1s}(\theta) & d_{2s}(\theta) & 0 & 0 & -d_{5s}(\theta) & d_{6s}(\theta) \\ 0 & 0 & -d_{3e}(\theta) & d_{4e}(\theta) & -d_{5e}(\theta) & d_{6e}(\theta) \end{pmatrix}^T \tag{13}$$

$$K_m = \text{diag.}\,[f_1(\alpha_1), f_2(\alpha_2), \cdots, f_6(\alpha_6)], \tag{14}$$

where $d_{ij}(\theta) > 0$ ($i = 1, 2, \ldots, 6$; $j = s, e$) is the length of the moment arm of muscle i to the shoulder (s) or elbow (e) joint; $f_i(\alpha_i) > 0$ is the stiffness of the muscle i; and diag. [ ] denotes the diagonal matrix. Also $\theta = (\theta_s, \theta_e)^T$ denotes the joint angle vector. Each row and column of the matrix G corresponds to each joint and muscle, respectively. Substituting (13), (14) into (11), we have each element of the joint stiffness matrix represented as

$$K_{ss} = d_{1s}^2(\theta) f_1(\alpha_1) + d_{2s}^2(\theta) f_2(\alpha_2) + d_{5s}^2(\theta) f_5(\alpha_5) + d_{6s}^2(\theta) f_6(\alpha_6), \tag{15}$$

$$K_{se} = d_{5s}(\theta) d_{5e}(\theta) f_5(\alpha_5) + d_{6s}(\theta) d_{6e}(\theta) f_6(\alpha_6), \tag{16}$$

$$K_{ee} = d_{3e}^2(\theta) f_3(\alpha_3) + d_{4e}^2(\theta) f_4(\alpha_4) + d_{5e}^2(\theta) f_5(\alpha_5) + d_{6e}^2(\theta) f_6(\alpha_6), \tag{17}$$

where K_{ss} and K_{ee} represent the shoulder and elbow components, respectively, and K_{se} denotes the coupling component between the shoulder and elbow joints.

In our experiment, the muscle activation levels were varied widely under the constant arm posture, so that the muscular effects to the arm impedance appears clearly.

Muscular Effects

The stiffness and viscosity of the muscle i is approximated by an N-th order polynomial of the corresponding muscle activation level, α_i:

$$f_i(\alpha_i) = \sum_{k=0}^{N} c_{ik}\, \alpha_i^k \qquad (18)$$

for all muscles, i = 1, 2, ..., 6. Substituting (18) into (15) - (17) yields a set of the N-th order polynomials for each element of the joint stiffness, since the moment arm of each muscle, $d_{ij}(\theta)$, can be considered as a constant for each muscle in our experiments.

Using the joint stiffness for ten data sets estimated in the experiments, which consist of five data sets measured in one day for each experiment, coefficients included in the polynomials were estimated by the standard least square method. **Tables 1** shows the estimated results for subject B with the ones for the joint viscosity. The joint viscoelasticity can be approximated by using the polynomial model of the muscle viscoelasticity with the appropriate order (more than N = 2) under the constant posture.

Figures 16 shows the accuracy of the predicted joint stiffness for the experimental results of subject B, where the vertical axis represents the joint stiffness and viscosity computed from the experimental results and the horizontal axis represents the ones predicted by using the second order polynomial model of the muscle viscoelasticity. The joint stiffness computed from the experimental results agrees with the predicted values.

Figure 17 shows the predicted changes of the hand stiffness ellipses with the activation levels of the single-joint muscles, where the activation levels of the flexors and the extensors are set to be $\alpha_1 = \alpha_3$ and $\alpha_2 = \alpha_4$, and the activation levels of the two -joint muscles used in the figure are $\alpha_5 = \alpha_6 = 0.1$. In the figure, the predicted changes of three parameters of the hand stiffness are shown as the 3D surfaces.

The measurements of the EMG signals and the joint angles are much easier than the estimation procedure of the hand impedance and can be performed without preventing movements of the subject. Therefore, the prediction of the hand impedance described here may be a useful technique for some purposes such as the control of the human-robot interactions and the analysis of skillful human movements in sports.

Table 1 Accuracy of fitting results of joint impedance

		K_{ss}	K_{se}	K_{ee}	B_{ss}	B_{se}	B_{ee}
$N=1$	R	0.595	0.645	0.917	0.796	0.609	0.891
	E	7218.09	4194.83	3056.50	15.58	7.94	5.59
$N=2$	R	0.739	0.649	0.944	0.855	0.616	0.914
	E	5064.28	4157.62	2077.05	11.43	7.83	4.47
$N=3$	R	0.841	0.661	0.948	0.874	0.629	0.918
	E	3261.07	4042.04	1931.65	10.06	7.64	4.25

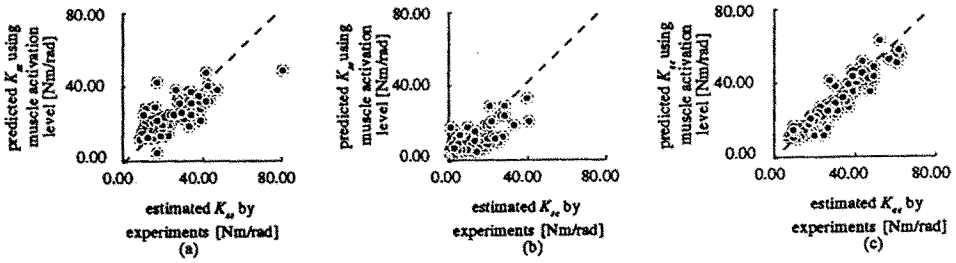

Fig. 16 Accuracy of predicted joint stiffness

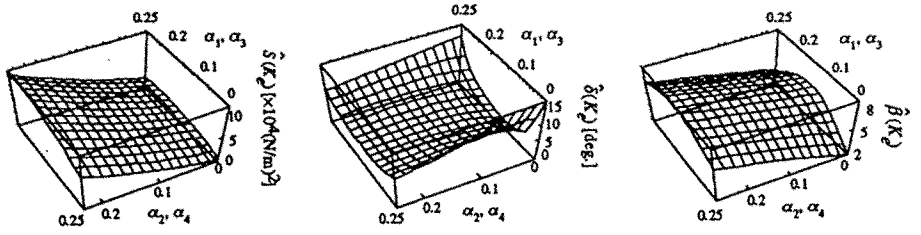

Fig. 17 Predicted changes of geometrical parameters of the hand stiffness ellipses

CONCLUSION

The purpose of this paper was to investigate the spatial characteristics of the hand impedance in multi-joint movements during isometric muscle contraction and to make clear the dependency on the muscle activity. The main results of the experiments can be summarized as follows: (1) geometrical parameters of the hand stiffness and viscosity ellipses change depending on the muscle activation levels of the subjects, (2) both the stiffness and the virtual equilibrium point of the subject's hand change depending on the amplitude of the generated hand force, (3) co-contraction of the flexor and the extensor increases the sizes of the hand stiffness and viscosity ellipses, and (4) hand stiffness and viscosity can be predicted from the joint angles and EMG signals of the subject's arm with a sufficient accuracy using polynomial models for the muscle viscoelasticity. The estimated impedance characteristics of the human arm can provide basic and important data for modeling and analysis of the multi-joint human arm movements. Also, the arm impedance model derived here should be useful for the control of human-robot interactions in which the impedance characteristics of human arm are often used as a model of a human operator.

In this paper, however, only the arm impedance in the steady-state of the muscle activation level and hand force have been analyzed. Future research will be directed to make clear how the arm impedance changes in the transient states of the muscle activation levels and to apply the arm impedance characteristics of human arm derived here to the control of human-robot interactions.

ACKNOWLEDGMENTS

The authors would like to thank to Prof. K. Ito, Prof. P. G. Morasso and Dr. M. Svinin for their helpful comments and discussions. This work has been supported in part by the scientific research foundation of the Ministry of Education, Culture and Science under Grant #07245103, "Research on Emerging Mechanism of Machine Intelligence."

REFERENCES

Mussa-Ivaldi, F. A., Hogan, N. and Bizzi, E., 1985, "Neural, mechanical and geometrical factors subserving arm posture in humans," Journal of Neuroscience, 5, 10, pp. 2732-2743

Flash, T. and Mussa-Ivaldi, F. A., 1990, "Human arm stiffness characteristics during maintenance of posture," Experimental Brain Research, 82, pp. 315-326

Dolan, J. M., Friedman, M. B. and Nagurka, L., 1993, "Dynamic and loaded impedance components in the maintenance of human arm posture," IEEE Transaction on System, Man, and Cybernetics, 23, 3, pp. 698-709

Tsuji, T., Goto, K., Moritani, M., Kaneko, M. and Morasso, P., 1994, "Spatial characteristics of human hand impedance in multi-joint arm movements," Proceedings of IEEE International Conference on Intelligent Robots and Systems, pp. 423-430

Tsuji, T., Morasso, P., Goto, K. and Ito, K., 1995, "Human hand impedance characteristics during maintained posture," Biological Cybernetics, 72, pp. 475-485

Dowben, R. M., "Contactility," *Medical Physiology*, ed. by V. B. Mountcastle and C. V. Mosby, 93 (1980).

Houk, J. C., 1979, "Regulation of Stiffness by Skeletomotor Reflexes," Ann. Rev. Physiol., pp. 99-104

Gomi, H., Koike, Y. and Kawato, M., 1992, "Human hand stiffness during discrete point-to-point multi-joint movement," Proceedings of the Annual International Conference of the IEEE Engineering in Medicine and Biology Society, pp. 1628-1629

Mussa-Ivaldi, F. A., 1986, "Compliance," in Human Movement Understanding, P. Morasso and V. Tagliasco (eds.), Elsevier, pp. 161-212